Electromagnetic Time-Reversal Imaging Using Grouped Sub-Arrays for Resolution Enhancements

Yuan-Qi Li [1], Xiang-Qian Zhang [1], and Ming-Yao Xia [2*]

[1] School of Electronic Engineering
University of Electronic Science and Technology of China, Chengdu, 611731, China
liyuanqiwangheng@163.com, xqzh@uestc.edu.cn

[2] School of Electronics Engineering and Computer Sciences
Peking University, Beijing, 100871, China
myxia@pku.edu.cn

Abstract ─ A new time-reversal (TR) imaging method using grouped sub-arrays for resolution enhancements is presented in this work. The method gives the image of the searching space for each target or scattering center at its own optimum instant, in contrast to the traditional TR imaging method that shows a snapshot of the whole domain at a specified instant. By introducing a grouping scheme that divides the time-reversal mirror (TRM) as many sub-TRMs, resolution enhancements in both cross-range and co-range directions are realized by means of destructive multiplication and incoherent superposition of the normalized sub-TRM imaging signals at non-target positions. The present method permits all targets or scattering centers to be rendered at equal visibility, and has no requirement on the number of transmitters. Several simulation examples are provided to examine the performance of the proposed method.

Index Terms ─ Grouped sub-arrays, imaging, resolution enhancement, signal normalization, time-reversal.

I. INTRODUCTION

Time-reversal (TR) technique was first proposed in acoustics [1,2], and latter extended to electromagnetic wave [3,4]. It lies on the invariance of the wave equations under time reversal operation in reciprocal and lossless media. It contains two stages. First, waves radiated from a source or scattered from a target are received and recorded by each element of an antenna array, called time-reversal mirror (TRM). Then, at each element, the recorded wave is time-reversed, i.e., in a first-in last-out way, and retransmitted into the same media. Space-time focusing of these retransmitted waves from individual elements will happen, i.e., they add coherently or achieve their maximum amplitude values synchronically at the original source or target position, but incoherently or non-synchronically at other positions.

For applications in wireless communications and wireless power transmission or combination, for which actual energy focusing is required, the retransmission and back-propagation must be taken place physically (physical TR) [5-7]. However, for applications in target locating or imaging, for which real energy focusing is not required, the back-propagation can be implemented synthetically or computationally (synthetic TR) [8-20]. This work is concerned with the target imaging by using the synthetic TR fashion.

The traditional TR imaging method is typically manipulated by synthetically back-propagating the time-reversed signals into the imaging domain and showing the image at the appropriate reference time "t=0" [10-12]. However, we may not know the t=0 reference precisely, or the t=0 reference may not be the optimal focusing instant. As revealed in [10], the traditional TR imaging method can locate point-like targets and extended perfectly electrical conducting (PEC) targets at the t=0 reference, but fails to locate the extended dielectric target at the same instant. The reason may be due to the multiple interior scattering, which amounts to a change of the original background medium. Another issue with the traditional TR imaging method is the near-far problem for imaging multiple targets [13], by which the farther or weaker targets are prone to be swamped by the nearer or stronger ones.

There exist other kinds of TR imaging methods based on the analyses of the time-reversal operator (TRO), including the decomposition operator of time-reversal (DORT) and the time-reversal multiple signal classification (TR-MUSIC) [11,14-20]. These methods can produce better imaging results, but their computing burden is heavily increased. Besides, these approaches demand that the number of targets or scattering centers cannot exceed the number of transmitters or receivers, which is somewhat inconvenient in applications.

Previously, we proposed a new TR imaging concept based on synchronism and illustrated with 2D targets

Submitted On: March 5, 2017
Accepted On: April 18, 2017

[21]. The purpose of this work is to present its extension to 3D case for practical applications, because real-world targets are 3D. We will show that the proposed algorithm would have much better imaging results than the traditional TR imaging method at the expense of a slightly increased computing load. Also, the present method should enjoy a significantly reduced computing cost than the DORT and TR-MUSIC methods, and get rid of the demand on the number of transmitters.

II. METHOD OUTLINE

Refer to Fig. 1. Consider a time-reversal imaging scenario in lossless and reciprocal medium. The receiving antennas or the time-reversal mirror (TRM) is deployed over the *xoy* plane, forming a planar array of size N_x by N_y. Their positions are known at $\mathbf{r}_n$ $(1 \le n \le N,\ N = N_x \times N_y)$. A point-like target is located at $\mathbf{r}_s$, which may be taken as an equivalent point current source with strength $\mathbf{J}_s(\mathbf{r},\omega) = \mathbf{P}_s(\omega)\delta(\mathbf{r}-\mathbf{r}_s)$. The radiating or scattering field from the target at the *n*-th antenna position is:

$$\mathbf{E}^s(\mathbf{r}_n,\omega) = \bar{\mathbf{G}}(\mathbf{r}_n,\mathbf{r}_s,\omega)\cdot[-j\omega\mu\mathbf{P}_s(\omega)], \quad (1)$$

where $\bar{\mathbf{G}}(\mathbf{r}_n,\mathbf{r}_s,\omega)$ is the dyadic Green's function from the target point $\mathbf{r}_s$ to the receiver at $\mathbf{r}_n$. If the polarization property of every antenna element is $\hat{q}$, say $\hat{q} = \hat{x}$, the received signal would be $S(\mathbf{r}_n,\omega) = \hat{q}\cdot\mathbf{E}^s(\mathbf{r}_n,\omega)$. After time-reversed, the signal can be taken as an equivalent point source with strength $\mathbf{J}_n(\mathbf{r},\omega) = \hat{q}(j\omega\varepsilon)S^*(\mathbf{r}_n,\omega)\delta(\mathbf{r}-\mathbf{r}_n)$ with $S^*(\mathbf{r}_n,\omega)$ being the complex conjugate of $S(\mathbf{r}_n,\omega)$. The reradiated field by the *n*-th antenna element is:

$$\mathbf{E}_n^{\mathrm{TR}}(\mathbf{r},\omega) = \bar{\mathbf{G}}(\mathbf{r},\mathbf{r}_n,\omega)\cdot[-j\omega\mu\mathbf{P}_n(\omega)], \quad (2)$$

where $\mathbf{P}_n(\omega) = \hat{q}(j\omega\varepsilon)S^*(\mathbf{r}_n,\omega)$. The imaging signal may be chosen to be a component of the retransmitted fields, i.e.,

$$S_{n,p}^{\mathrm{TR}}(\mathbf{r},\omega) = \hat{p}\cdot\mathbf{E}_n^{\mathrm{TR}}(\mathbf{r},\omega),\ 1\le n\le N, \quad (3)$$

where $\hat{p}$ stands for a chosen polarization direction, say $\hat{p} = \hat{x}$. Converted into time domain, the imaging signals are denoted by $s_{n,p}^{\mathrm{TR}}(\mathbf{r},t)$ $(1\le n\le N)$. According to the time reversal focusing principle, these imaging signals will achieve their maximum amplitude values synchronically at the target position $\mathbf{r} = \mathbf{r}_s$, but non-synchronically at any non-target position $\mathbf{r} \ne \mathbf{r}_s$. The traditional TR imaging method shows a snapshot of the summed signal, i.e.,

$$I(\mathbf{r}) = \sum_{n=1}^{N} s_n^{\mathrm{TR}}(\mathbf{r},t_{\mathrm{ref}}), \quad (4)$$

where t_{ref} is a reference time that the snapshot is taken, which is usually set to be 0. This traditional approach has good performance for a single target, except that the resolution cannot beat the diffraction limit. However, if multiple targets are present, the traditional method may suffer: (i) farther or weaker targets are prone to be swamped by nearer or stronger ones; (ii) there may not exist an optimal t_{ref} for all targets or scattering centers to be appropriately rendered in one snapshot or image.

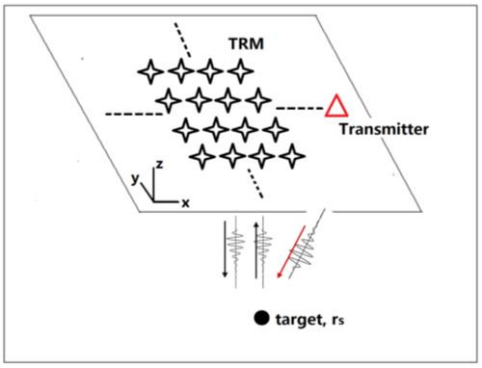

Fig. 1. Time-reversal imaging configuration.

To overcome the two problems mentioned above and improve the resolutions, a new TR imaging algorithm is proposed as follows.

(i) Divide the TRM into many sub-TRMs and construct the sub-TRM signals by:

$$u_m(\mathbf{r},t) = \sum_{l=0}^{L-1} s_{m+l}^{\mathrm{TR}}(\mathbf{r},t),\ 1\le m\le M, \quad (5)$$

where M is the total number of sub-TRMs, and L is the number of antenna elements in each sub-TRM. The *m*-th sub-TRM starts from the *m*-th antenna element, which includes L_x elements in the *x*-direction and L_y elements in the *y*-direction, so that $L = L_x \times L_y$. Specifically, the 1-st sub-TRM is a rectangular array associated with the corner elements (1,1) and (L_x, L_y). The last sub-TRM is associated with the corner elements $(N_x - L_x + 1, N_y - L_y + 1)$ and (N_x, N_y). It is clear that $M = (N_x - L_x + 1)\times(N_y - L_y + 1)$.

(ii) Normalize all the sub-TRM signals by:

$$\bar{u}_m(\mathbf{r},t) = \frac{u_m(\mathbf{r},t)}{u_m(\mathbf{r},t_m(\mathbf{r}))},\ 1\le m\le M, \quad (6)$$

where $t_m(\mathbf{r})$ is the time that makes $u_m(\mathbf{r},t)$ to achieve its maximum amplitude value at the imaging point $\mathbf{r}$. At all target positions $\mathbf{r} = \mathbf{r}_k$ $(1\le k\le K,\ K$ is the number of targets), the $t_m(\mathbf{r}_k)$ is almost independent of the index *m*, that is, all the normalized signals would synchronically achieve their maximum amplitude value 1. At any non-target position $\mathbf{r} \ne \mathbf{r}_k$, $t_m(\mathbf{r})$ is dependent on *m*, so that the normalized signals cannot synchronically achieve their maximum amplitude value 1. The normalization would allow all potential targets or scattering centers to

be shown at equal visibility to avoid swamping of farther or weaker targets by nearer or stronger ones.

(iii) To enhance the synchronism of the normalized signals at each target position and non-synchronism at any non-target position, a multiplicative signal is defined as:

$$U(\mathbf{r},t)=\prod_{m=1}^{M}\bar{u}_m(\mathbf{r},t)\,. \tag{7}$$

This manipulation would substantially improve the cross-range resolution. As a result, locating all the targets is possible by searching the positions for $U(\mathbf{r},t)$ to achieve its maximum amplitude values, which should be 1 in theory at all target positions. However, a threshold value *val* may be specified and a target is recognized if the multiplied signal is greater than the threshold. For instance, if $U(\mathbf{r}_k,t_0(\mathbf{r}_k))\ge val$, a target at $\mathbf{r}=\mathbf{r}_k$ would be recognized and the optimum moment to observe this target is $t_0(\mathbf{r}_k)$.

(iv) To alleviate the negative influence of the normalization and improve the co-range resolution, taking further advantage of the synchronism is possible. Hence, we define the final image by means of the superposition of the images $U(\mathbf{r},t_0(\mathbf{r}_k))$ $(1\le k\le K)$ that are in favor to show all targets as:

$$I(\mathbf{r})=\sum_{k=1}^{K}U(\mathbf{r},t_0(\mathbf{r}_k)). \tag{8}$$

This step would significantly enhance the co-range resolution.

III. SIMULATION VALIDATION

In this section, we provide several examples to examine the performance of the proposed method. They include one point target, two point targets at different distance, two extended targets with different scattering properties, and one point target in multiple clutters.

The simulation scenario is shown in Fig. 1. The TRM is made up of $N=N_x\times N_y=9\times 9=81$ elements, each of which is an *x*-polarized dipole. The array's pitch in both *x*- and *y*-directions is half of the center wavelength $\lambda_c/2$ of the excitation wave, which is taken to be the modulated Gaussian pulse with the center frequency at $f_c=4\,\text{GHz}$ ($\lambda_c=7.5\,\text{cm}$) and the effective bandwidth $\Delta f=4\,\text{GHz}$ ($\lambda_{\min}=5\,\text{cm}$). Only one transmitter is used in the following simulations, which is placed at $(3\lambda_c,0,0)$. The imaging domain is a cube of size $4\lambda_c\times 4\lambda_c\times 4\lambda_c$, from $-2\lambda_c$ to $2\lambda_c$ in both *x*- and *y*-directions, and from $-8\lambda_c$ to $-4\lambda_c$ in *z*-direction. FDTD method is used to perform the calculations for wave radiation, propagation and scattering. The computing domain, including the perfectly matched layers (PML), is a square cylinder with base side size $6\lambda_c$ or 45 cm and height $9\lambda_c$, which is meshed with a spatial cell size $\Delta x=\Delta y=\Delta z=0.375\,\text{cm}$.

A. One point target

For this example, we choose $L_x=L_y=1$, so that a total of $M=9\times 9=81$ sub-TRMs is formed. One point-like target is placed at $(0,0,-6\lambda_c)$. The 3D image is sown in Fig. 2, and its projections onto the *xoy*, *yoz* and *xoz* planes, respectively, are shown in Fig. 3. For comparison, the image obtained by using the traditional TR imaging method is also projected onto the *xoy*, *yoz* and *xoz* planes, respectively, as shown in Fig. 4. To have a close look, a comparison of the relative image values in the *x*- and *z*-directions is shown in Fig. 5. It is obvious that our new method has much higher resolutions in both directions than the traditional approach.

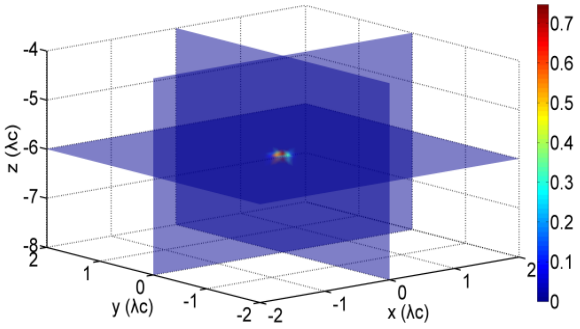

Fig. 2. Time-reversal imaging result for one point-like target by the proposed method.

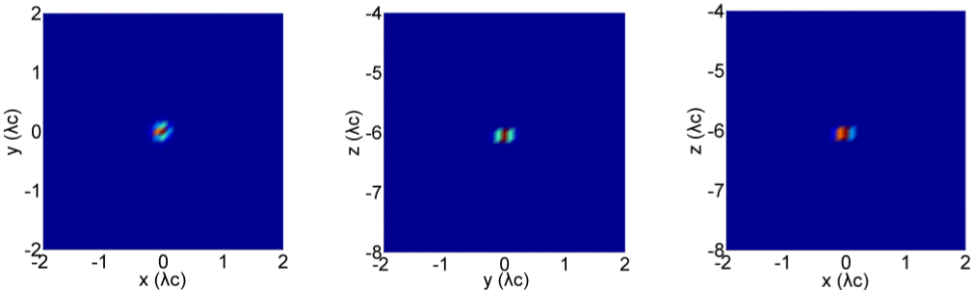

Fig. 3. The projections of Fig. 2 onto the *xoy*, *yoz*, *xoz* planes (from left to right), respectively.

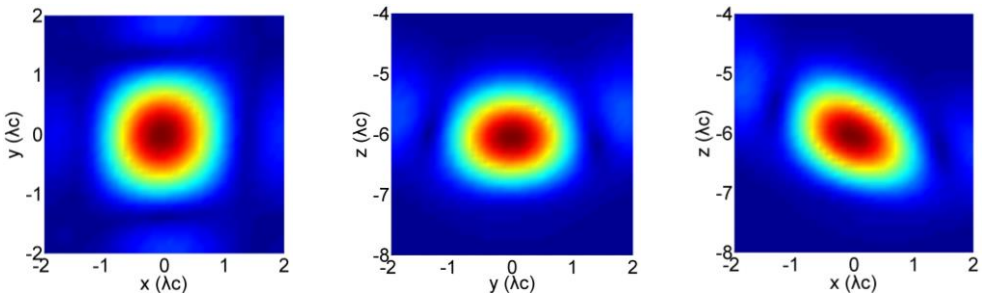

Fig. 4. The imaging results of one point-like target by the traditional method projected onto the *xoy*, *yoz*, *xoz* planes (from left to right), respectively.

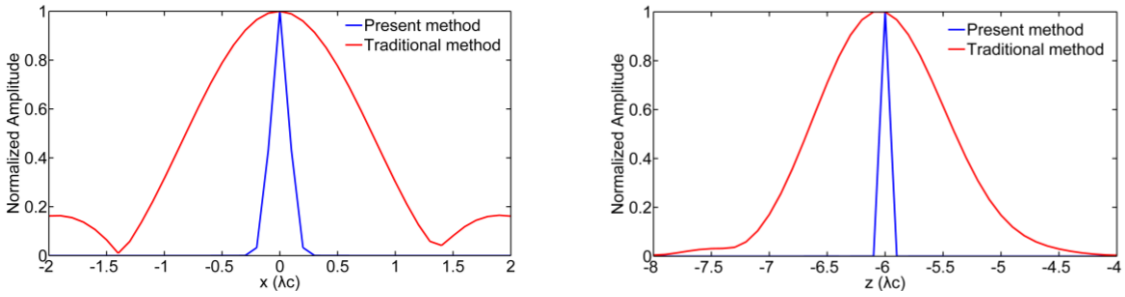

Fig. 5. Comparison of resolutions in terms of normalized amplitude values in the cross-range (left) and co-range (right) directions between the two algorithms: the present method (blue line) and the traditional method (red line).

B. Two targets at different distance

We choose $L_x = L_y = 3$ in this example, so that we get $M = 7 \times 7 = 49$ sub-TRMs. The two point-like targets are placed at $(0,0,-5\lambda_c)$ and $(0,0,-7\lambda_c)$, respectively. The projections of the image onto the *xoy*, *yoz* and *xoz* planes, respectively, are shown in Fig. 6. It is verified that both targets are almost equally well located. However, by using the traditional method, the target at the farther place is seriously degraded as shown in Fig. 7.

C. Two extended targets with different scattering properties

In this example, the simulation configuration is the same as the previous example, except that the two point-like targets are replaced by two extended spherical targets with a radius of $\lambda_c / 4$, centering at $(0,0,-7\lambda_c)$ and $(0,0,-5\lambda_c)$, respectively. The former is made of PEC, and the latter is made of dielectric material $\varepsilon_r = 3$.

The imaging result by the proposed method after being projected onto the *xoy*, *yoz* and *xoz* planes, respectively, is shown in Fig. 8. It is apparent that there are two targets in the imaging space and each target has three prominent scattering centers. However, by using the traditional method, as shown in Fig. 9, it seems hard to judge that there are two targets there. It looks that there are three targets, or there is only one target with three scattering centers.

D. One target in multiple clutters

In this last example, the simulation configuration is shown Fig. 10. But we choose $L_x = L_y = 1$ here, so that the number of sub-TRMs is equal to the number of the whole antenna elements, which is 81. One point-like target as indicated in green is located at $(0,0,-6\lambda_c)$, around which there are eight extended spherical clutters, whose radius is $\lambda_c / 4$, as indicated in yellow. First, the scattered field by the clutters in the absence of the target is calculated. Then the scattered field in the presence of the target is re-calculated. The difference field at each antenna element between the two cases is used for imaging of the target. The 3D imaging result is shown in Fig. 11. It is seen that good agreement between the actual and the constructed target is observed.

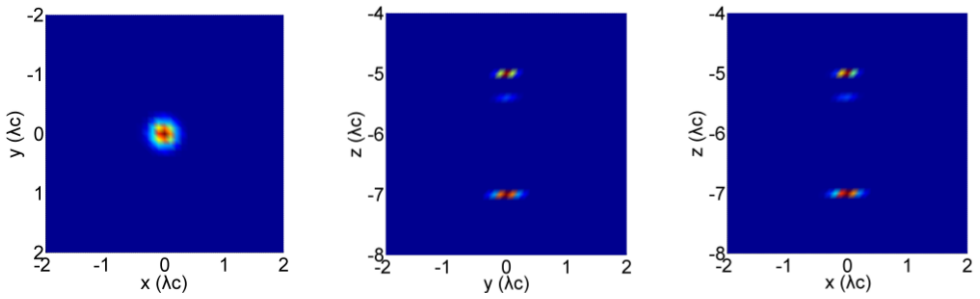

Fig. 6. The imaging results for two point-like targets by the present method projected onto the *xoy*, *yoz*, *xoz* planes (from left to right), respectively.

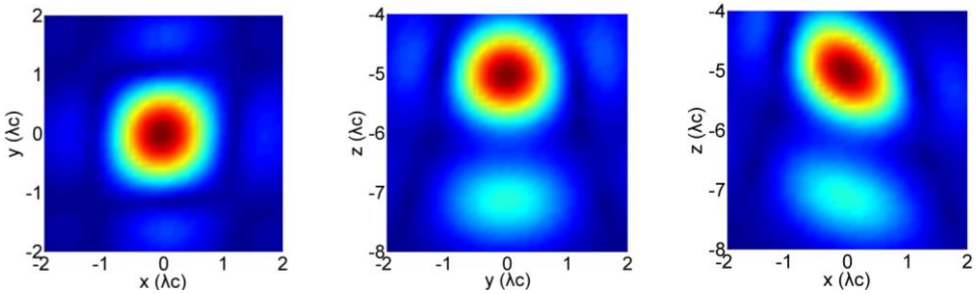

Fig. 7. The imaging results for two point-like targets by the traditional method projected onto the *xoy*, *yoz*, *xoz* planes (from left to right), respectively.

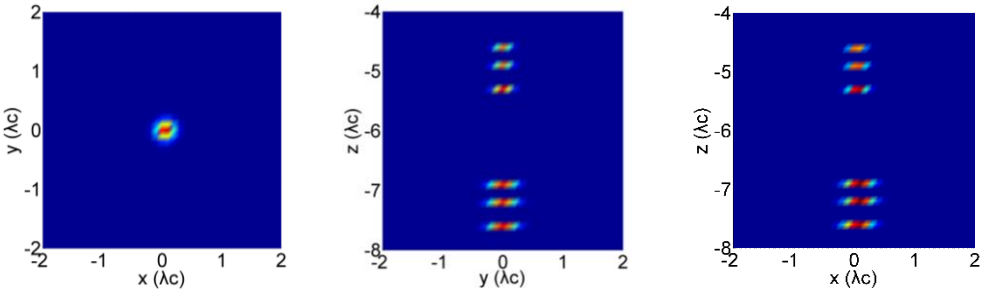

Fig. 8. The imaging results for two extended targets by the present method projected onto the *xoy*, *yoz*, *xoz* planes (from left to right), respectively.

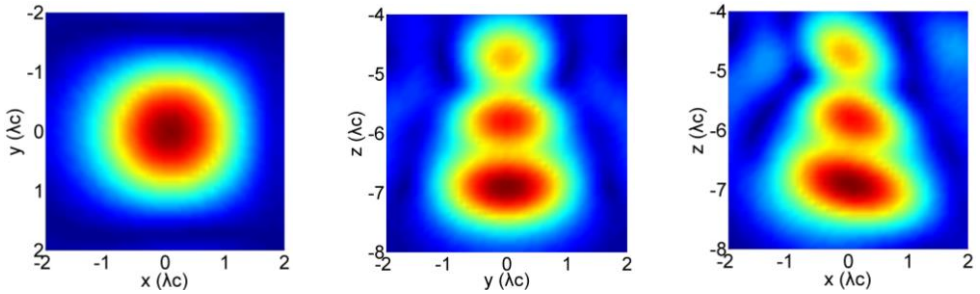

Fig. 9. The imaging results for two extended targets by the traditional method projected onto the *xoy*, *yoz*, *xoz* planes (from left to right), respectively.

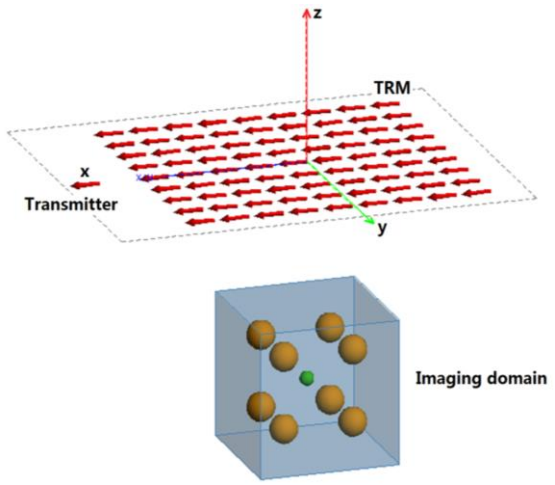

Fig. 10. Simulation configuration for imaging of one point-like target (denoted by a green sphere) in several clutters (denoted by eight yellow spheres).

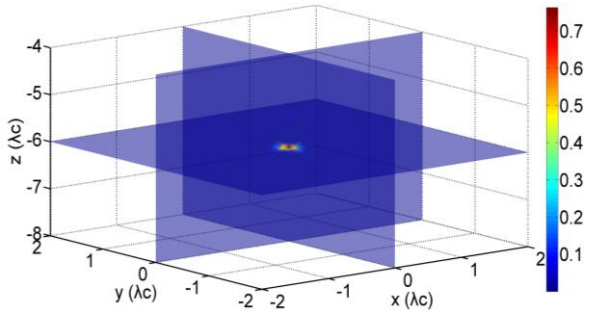

Fig. 11. Time-reversal imaging result for one point-like target situated at $(0,0,-6\lambda_c)$ in the presence of eight extended clutters.

IV. CONCLUDING REMARKS

A new time-reversal imaging method for 3D targets is proposed by making full use of the synchronism that the retransmitted signals from the TRM elements achieve their maximum amplitude values synchronically at target positions but non-synchronically at non-target positions. Implementation of the method is composed of four steps: (i) Grouping of the retransmitted signals, by which the synchronism is maintained for further processing; (ii) Normalization of the sub-TRM signals, by which all targets would be shown at equal visibility to avoid masking; (iii) Multiplication of the normalized signals, by which the cross-range resolution would be greatly enhanced; and (iv) Superposition of the images that are optimum for observation of individual targets, by which all targets would be rendered in one frame with substantially improved co-range resolution. Simulation examples show that the proposed method has satisfying performance in discriminating multiple targets or scattering centers. Further investigation of the method in noisy environment is in progress.

ACKNOWLEDGMENT

This work was supported by the NSFC Projects 61531001 and 61271032.

REFERENCES

[1] M. Fink, "Time reversal of ultrasonic fields-Part I: Basic principles," *IEEE Trans. Ultrason., Ferroelectr., Freq. Control*, vol. 39, pp. 555-566, 1992.

[2] D. Cassereau and M. Fink, "Time-reversal of ultrasonic fields-Part III: Theory of the closed time-reversal cavity," *IEEE Trans. Ultrason., Ferroelectr., Freq. Control*, vol. 39, pp. 579-592, 1992.

[3] G. Lerosey, J. De Rosny, A. Tourin, A. Derode, G. Montaldo, and M. Fink, "Time reversal of electromagnetic waves," *Phys. Rev. Lett.*, vol. 92, pp. 193904, 2004.

[4] G. Lerosey, J. De Rosny, A. Tourin, A. Derode, and M. Fink, "Time reversal of wideband microwaves," *Applied Phys. Lett.*, vol. 88, pp. 154101, 2006.

[5] H. T. Nguyen, J. B. Andersen, G. F. Pedersen, P. Kyritsi, and P. C. F. Eggers, "Time reversal in wireless communications: A measurement- based investigation," *IEEE Trans. Wireless Commun*., vol. 5, no. 8, pp. 2242-2252, Aug. 2006.

[6] H. El-Sallabi, P. Kyritsi, A. Paulraj, and G. Papanicolaou, "Experimental investigation on time reversal precoding for space-time focusing in wireless communications," *IEEE Trans. Instrumentation and Measurement*, vol. 59, no. 6. pp. 1537-1543, 2010.

[7] M. L. Ku, Y. Han, H. Q. Lai, Y. Chen, and K. J. R. Liu, "Power waveforming: Wireless power transfer beyond time reversal," *IEEE Trans. Signal Processing*, vol. 64, no. 22, pp. 5819-5834, 2016.

[8] A. B. Gorji and B. Zakeri, "Time-reversal through-wall microwave imaging in rich scattering environment based on target initial reflection method," *Applied Computational Electromagnetics Society Journal*, vol. 30, no. 6, pp. 626-637, 2015.

[9] B. Li, "Noise suppression detection method based on time reversed signal waveform similarity," *Applied Computational Electromagnetics Society Journal*, vol. 32, no. 2, pp. 141-146, 2017.

[10] D. H. Liu, G. Kang. L. Li, Y. Chen, S. Vasudevan, W. Joines, Q. H. Liu, J. Krolik, and L. Carin, "Electromagnetic time-reversal imaging of a target in a cluttered environment," *IEEE Trans. Antennas Propag*., vol. 53, pp. 3058-3066, Sep. 2005.

[11] M. E. Yavuz and F. L. Teixeira, "Full time-domain DORT for ultrawideband fields in dispersive,

random inhomogeneous media," *IEEE Trans. Antennas Propag.*, vol. 54, pp. 2305-2315, Aug. 2006.

[12] A. E. Fouda and F. L. Teixeira, "Statistical stability of ultrawideband time-reversal imaging in random media," *IEEE Trans. Geosci. Remote Sensing*, vol. 52, no. 2, pp. 870-879, Feb. 2014.

[13] G. Shi and A. Nehorai, "A relationship between time-reversal imaging and maximum likelihood scattering estimation," *IEEE Trans. Signal Process.*, vol. 55, no. 9, pp. 4707-4711, Sep. 2007.

[14] C. Prada, S. Mannevile, D. Spoliansky, and M. Fink, "Decomposition of the time reversal operator: Detection and selective focusing on two scatterers," *J. Acoust. Soc. Am.*, vol. 99, pp. 2067-2076, 1996.

[15] H. Lev-Ari and A. J. Devaney, "The time reversal techniques reinterpreted: Subspace-based signal processing for multistatic target location," *Proc. IEEE Sensor Array Multichanneal Signal Process. Workshop*, pp. 509-513, 2000.

[16] A. J. Devaney, "Super-resolution processing of multi-static data using time reversal and MUSIC," Unpublished paper, available from the author's web site. http://www.ece.neu.edu/fac-ece/devaney/ajd/preprints.htm

[17] M. E. Yavuz and F. L. Teixeira, "Ultra-wideband microwave sensing and imaging using time-reversal techniques: A review," *Remote Sens.*, vol. 1, no. 3, pp. 466-495, 2009.

[18] M. E. Yavuz and F. L. Teixeira, "Space-frequency ultrawideband time-reversal imaging," *IEEE Trans. Geosci. Remote Sens.*, vol. 46, pp. 1115-1124, 2008.

[19] S. Bahrami, A. Cheldavi, and A. Abdolali, "Ultrawideband time-reversal imaging with frequency domain sampling," *IEEE Geosci. Remote Sens. Lett.*, vol. 11, no. 3, pp. 597-601, 2014.

[20] X. M. Zhong, C. Liao, and W. B. Lin, "Space-frequency decomposition and time-reversal imaging," *IEEE Trans. Antennas Propag.*, vol. 63, no. 12, pp. 5619-5628, 2015.

[21] Y. Q. Li and M. Y. Xia, "Target location based on time focusing of time-reversal retransmitting signals," *IEEE Inter. Geosci. Remote Sensing Sym.*, Milan, Italy, pp. 3149-3151, July 2015.

Yuan-Qi Li was born in Sichuan, China, in 1988. He received the M.Sc. degree from the School of Electronic Engineering, University of Electronic Science and Technology of China, Chengdu, China, in 2012, and is currently a Ph.D. student at the same school. His research area is on computational electromagnetics and applications, especially on object detection and imaging.

Xiang-Qian Zhang was born in Shanxi, China, in 1976. He received the M.Sc. degree from the School of Optoelectronic Information, the University of Electronic Science and Technology of China (UESTC), Chengdu, China, in 2005. Currently, he is an Engineer with the School of Electronic Engineering, UESTC. His research interests include microwave antennas, computational electromagnetics and applications, and electromagnetic scattering imaging.

Ming-Yao Xia was born in Jiangxi, China, in 1963. He received the M.Sc. and Ph.D. degrees in Electrical Engineering from the Institute of Electronics, Chinese Academy of Sciences (IECAS), in 1988 and 1999, respectively. From 1988 to 2002, he was with IECAS as an Engineer and a Senior Engineer. He was a Visiting Scholar at the University of Oxford, UK, from October 1995 to October 1996. From June 1999 to August 2000 and from January 2002 to June 2002, he was a Senior Research Assistant and a Research Fellow, respectively, with the City University of Hong Kong. He joined Peking University (PKU) as an Associate Professor in 2002 and was promoted to Full Professor in 2004. He moved to the University of Electronic Science and Technology of China (UESTC) as a Chang-Jiang Professor nominated by the Ministry of Education of China in 2010. He returned to PKU after finishing the appointment in 2013. He was a recipient of the Young Scientist Award of the URSI in 1993. He was awarded the First-Class Prize on Natural Science by the Chinese Academy of Sciences in 2001. He was the recipient of the Foundation for Outstanding Young Investigators presented by the National Science Foundation of China (NSFC) in 2008. He was an Associate Editor of the IEEE Transactions on Antennas and Propagation. His research interests include electromagnetic theory, computational electromagnetics and applications, microwave antennas and components, microwave scattering remote sensing, and electromagnetic detection and imaging.